Subsurface model inversion: pushing the limits of resolution

Musa Maharramov and Biondo L. Biondi

ABSTRACT

Detecting and inverting the imprint of changing subsurface elastic parameters on seismic data lies at the heart of time-lapse seismic imaging for reservoir monitoring. In this work we demonstrate that the recently proposed technique of simultaneous time-lapse full-waveform inversion with a model-difference regularization can be used to extract high-resolution information on magnitude and location of subsurface velocity and stress anomalies, potentially providing valuable input for reservoir monitoring and assessment of geohazards.

INTRODUCTION

Fluid movement in the subsurface and the associated changes in saturation translate into changes of the subsurface elastic parameters. Stress changes, whether due to fluid extraction/injection or deformation (such as slips on preexisting faults) affect the elastic parameters as well. Detecting and inverting the imprint of changing subsurface elastic parameters on seismic data is key to time-lapse seismic imaging for reservoir monitoring (Johnston, 2013). A recently developed methodology for time-lapse full-waveform inversion (FWI) based on a simultaneous inversion with a total-variation (TV) model-difference regularization (Maharramov et al., 2015, 2016) has been demonstrated to achieve multi-scale inversion of subsurface changes in the presence of strong repeatability issues. The main objective of this work is to demonstrate that even the weakest subsurface changes can still be recovered by the joint full-waveform inversion with regularization. More specifically, using a synthetic example with added noise, we demonstrate that reliable indicators of the subsurface stress change and location of the stress anomaly can be extracted from seismic data. Moreover, relative magnitudes of the inverted model changes at various vintages represent the actual relative changes. We discuss the implications of this observation for reservoir monitoring and seismic hazard assessment.

A change of the subsurface stress field (more specifically, change of the effective stress) results in changes of the acoustic velocity (Johnston, 2013). The following empirical relation is often used to describe this dependence in reservoir rocks,

$$V \;=\; V_\infty \left(1 - A \exp -\frac{P}{P_0}\right), \tag{1}$$

The reproducibility of the results presented in this article will be tested by the end of May 2017.

where V is acoustic velocity, P is *isotropic* effective stress, and V_∞, A, P_0 are positive fitting constants for various types of rocks (Domenico, 1977; Zimmer, 2003; Lee, 2003; Johnston, 2013)—see Figure 1. Equation (1) means that velocities increase in "compacting" rocks with increasing effective stress, flattening out at high effective stress—see, for example, Figure 20 from Chapter 3 of Johnston (2013). Typically, a few megapascal change in the effective stress results in a few tens of meters per second change in the acoustic velocity within the affected rocks. The evolution of subsurface elastic moduli in response to changes in the effective isotropic stress as a result of compaction of pore pressure change is a central topic of seismic time-lapse analysis, and the subject of continuing active research. Going beyond the effects of isotropic stress change, the effects of shear strain on the elastic properties of granular and clay-rich layered materials (for example, expected compositions of fault gouges) may be quite significant (Knuth et al., 2013), potentially allowing us to study the evolution of tectonic fault zones using time-lapse seismic.

Successfully applying time-lapse seismic to the analysis of subtle subsurface deformation effects requires pushing the limits of resolution. Can relatively small changes of the acoustic and elastic velocities be detected from seismic data? We show that the simultaneous FWI with a sparsity-promoting model-difference regularization can indeed reliably resolve such small changes in the presence of noise.

THEORY

In the first subsection we describe some of the key geomechanical models that govern the effect of subsurface deformation on the elastic moduli, and propose a computational framework for integrating such models with seismic inversion. In the second subsection we conduct a resolution analysis of our proposed multi-scale FWI technique.

Sensitivity of elastic moduli to stress

Experimentally obtained empirical trends of equation (1) and Figure 1 provide the most direct way of relating the effective stress and seismic velocities. However, theoretical rock physics models may still provide a useful and powerful tool in combination with seismic inversion. For the P-wave and S-wave velocities we have

$$V_P = \sqrt{\frac{K + 4/3\mu}{\rho}}, \quad V_S = \sqrt{\frac{\mu}{\rho}}, \tag{2}$$

where K, μ, and ρ are the bulk and shear rock moduli, and ρ is the rock density. A simple rock model based on an elastic sphere pack subject to confining pressure is given by the Hertz-Mindlin theory (Mindlin, 1949; Mavko et al., 2009), which yields

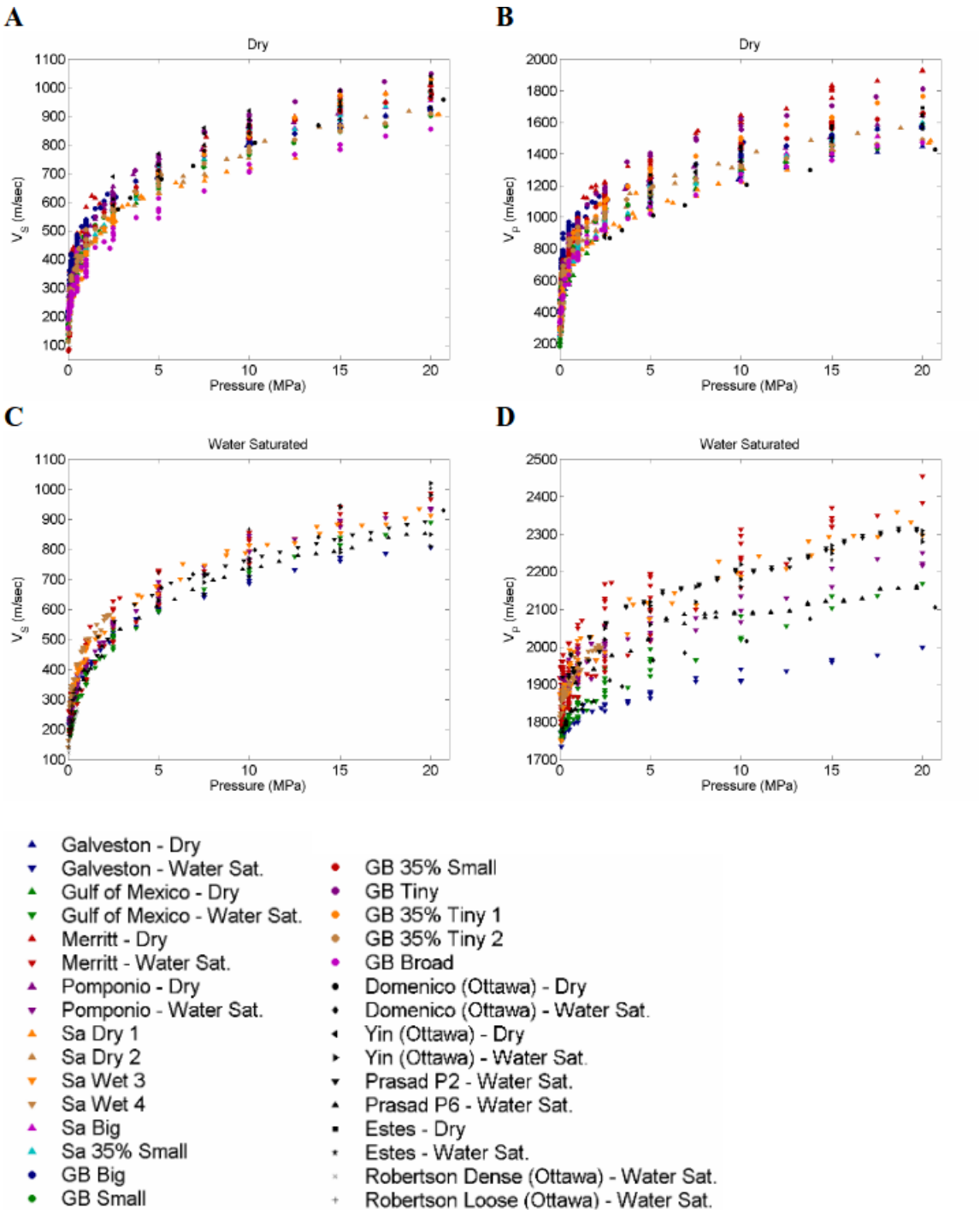

Figure 1: Experimental velocity measurement results and comparison presented by Zimmer (2003) (reproduced from Figure 2.9 of Zimmer (2003)). Laboratory measurements by Zimmer (2003) compared to measurements made on clean sands by Domenico (1977), Prasad and Domenico (1992), Yin (1992), Estes et al. (1994), and Robertson et al. (1995): A) dry shear-wave velocities, B) dry compressional-wave velocities, C) water-saturated shear-wave velocities, and D) water-saturated compressional wave velocities. [**NR**]

the following expressions for the dry rock elastic moduli:

$$K_{HM} \;=\; \sqrt[3]{\frac{n^2(1-\phi)^2\mu}{18\pi^2(1-\nu)^2}P}, \tag{3}$$

$$\mu_{HM} \;=\; \frac{5-4\nu}{5(2-\nu)}\sqrt[3]{\frac{3n^2(1-\phi)^2\mu}{2\pi^2(1-\nu)^2}P}, \tag{4}$$

where μ and ν are the solid phase shear modulus and Poisson ratio; P is the effective stress; ϕ is the depositional porosity, and n is the coordination number (the average number of contacts per grain) empirically estimated from porosity by the Murphy equation (Avseth et al., 2005),

$$n \;=\; 20 - 34\phi + 14\phi^2. \tag{5}$$

The Gassmann fluid substitution equations can then be used to obtain the bulk modulus of a fluid-saturated rock (Mavko et al., 2009). Rock density in (2) is obviously always an arithmetic mean of the constituent densities.

Equations (2-5) provide simple analytical relations between the seismic velocities on the one hand, and the effective stress, porosity and solid phase moduli, on the other hand. Such relations can be used, in principle, to invert the effective stress from seismic data. However, this simplicity is misleading as the Hertz-Mindlin theory describes an extreme example of a single-mineral sphere packing. However, it may still provide an adequate description of a single constituent part of a composite rock. Estimating the elastic moduli of a sediment from its constituent parts depends on the sequence of depositions, diagenesis and compaction (Mavko et al., 2009) that formed the sediment. For example, a simple harmonic (Reuss) average (Avseth et al., 2005) can be used for estimating the composite moduli of unconsolidated rocks and suspensions. A more realistic compositional model is provided by the Hashin-Shtrikman bounds (Hashin and Shtrikman, 1963; Mavko et al., 2009),

$$K_{HS} = K_1 \;+\; \frac{f_2}{(K_2-K_1)^{-1} + f_1(K_1+4\mu_1/3)^{-1}}, \tag{6}$$

$$\mu_{HS} = \mu_1 \;+\; \frac{f_2}{(\mu_2-\mu_1)^{-1} + 2f_1(K_1+2\mu_1)\left[5\mu_1(K_1+4\mu_1/3)\right]^{-1}}, \tag{7}$$

where $K_{1,2}$ and $\mu_{1,2}$ are the bulk and shear moduli of the two phases, and $f_{1,2}$ are the volume fractions of the individual phases. Equations (6,7) are obtained from a theoretical model of a composite rock schematically depicted in Figure 2 from Mavko et al. (2009). The second material forms the darker core spheres, and the first material forms the lighter outer shells. Volume fractions of the shells and cores are f_1 and f_2, respectively. The model assumes that spheres of arbitrarily small sizes completely fill up the entire space.

in combination with the Gassmann fluid substitution equations
that assumes constant stress in all constituent parts

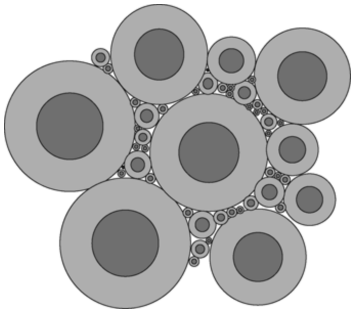

Figure 2: Physical interpretation of the Hashin-Shtrikman bounds for the bulk modulus of a two-phase material (reproduced from Figure 4.1.2 of Mavko et al. (2009)). [**NR**]

Avseth et al. (2016) used the Hertz-Mindlin theory, Gassmann fluid substitution and nested Hashin-Shtrikman bounds to express the acoustic velocity as a function of the effective stress in patchy, poorly to moderately consolidated sands. The resulting acoustic velocity models were used to estimate seismic time-shifts due to reservoir compaction and production at an offshore field using the following vertical traveltime approximation,

$$\Delta\tau \;=\; 2\int_{z_0}^{z_1} \left(s_b^P - s_m^P\right) dz, \tag{8}$$

where z_0 and z_1 are the reservoir top and bottom depths, and s_b^P and s_m^P are the baseline and monitor acoustic slowness models. Avseth et al. (2016) then used (8) to invert effective stress changes within the reservoir from observed time shifts.

We demonstrate in the subsequent sections that time-lapse FWI with a model-difference regularization can achieve a stable resolution of small velocity anomalies. Instead of using the equation (8), we propose to use FWI *simultaneously* with equations (2-7) to produce spatially variable estimates of stress changes. While quantitative accuracy of time-lapse FWI may be limited due to, for example, aggressive model-difference regularization, relative magnitudes of velocity changes and their *spatial heterogeneity* can still be well recovered (Maharramov and Biondi, 2017), leading to a new FWI technique of heterogeneous relative stress-change inversion.

So far we have been focusing on the effect of isotropic stress on seismic velocities. However, important geomechanical models of earth deformation, such as the antiplane stress model of an infinite strike-slip fault (Segall, 2010), involve only shear strains. Our ability to observe and measure a build-up of shear stress energy near seismogenic fault zones as a result of interseismic deformation is key to the timely assessment of geohazards. There is a growing body of evidence that suggests that both the velocities and amplitudes of transmitted acoustic and shear waves are affected by shear strains. While we are unaware of any theoretical rock physics models for predicting the evolution of elastic moduli under shear strain, the latest experimental results involving granular/clay mixtures typical for fault gouges (Knuth et al., 2013) point to significant measurable effects of shear strain on the acoustic velocity (see Figure 3).

These results imply that high-resolution time-lapse seismic inversion may be able to detect shear deformation—for example, near fault gouges. This information may potentially provide insights into the micromechanics at the fault interface that control

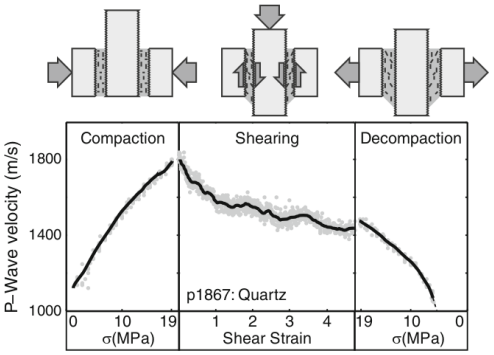

Figure 3: A V_P versus shear strain (middle panel) dependence obtained by Knuth et al. (2013) for granular .1-1 cm thick quartz layers with $\approx 100\mu m$ grain sizes (reproduced from Figure 5 of Knuth et al. (2013)). [**NR**]

earthquake nucleation and rupture propagation.

Multiscale subsurface model inversion

In our method, we invert the baseline and monitor models *simultaneously* by solving the following optimization problem:

$$\text{minimize } \alpha \| \exp i\arg \mathbf{u}_b - \exp i\arg \mathbf{d}_b \|_2^2 + \beta \| \exp i\arg \mathbf{u}_m - \exp i\arg \mathbf{d}_m \|_2^2 + \quad (9)$$

$$\delta \|\mathbf{WR}(\mathbf{m}_m - \mathbf{m}_b)\|_1 \quad (10)$$

with respect to both the baseline and monitor models $\mathbf{m}_b$ and $\mathbf{m}_m$. Problem (9,10) describes a time-lapse FWI with a model difference regularization (10) (Maharramov et al., 2015); $\mathbf{d}_b$ and $\mathbf{d}_m$ are the observed baseline and monitor data; $\mathbf{u}_b$ and $\mathbf{u}_m$ are the predicted baseline and monitor data; $\mathbf{W}$ denotes an optional weighting operator. When $\mathbf{R} = \nabla$, the regularization or "model-styling" term (10) represents a *total-variation (TV) regularization* that promotes "blockiness" of the model-difference, potentially reducing oscillatory artifacts (Rudin et al., 1992). If $\mathbf{R} = \mathbf{I}$ is the identity map, we obtain a sparsity-promoting L_1 model-difference regularization. Problems with $\mathbf{R} = \nabla$ and $\mathbf{R} = \mathbf{I}$ can be solved in a cascaded fashion, resolving "blocky" changes first, followed by spiky velocity-difference anomalies (Maharramov et al., 2016). The data misfit terms (9) are formulated in the frequency domain and represent misfits between the amplitude-normalized observed and predicted wave fields at different vintages, in other words representing phase misfits. Maharramov et al. (2016) showed that minimization of the phase misfits in (9) is to a first order and under the travel-time approximation equivalent to a tomographic inversion of travel-time delays due to changes in the subsurface model. Once the tomographic (background-velocity) component has been resolved, spiky or oscillatory components that may represent amplitude effects can be resolved by replacing the phase-only misfits (9) with the conventional phase-and-amplitude L_2 misfits (Maharramov et al., 2016). However, in this work we focus on a tomographic inversion of time-lapse effects that can be observed in minuscule time-shifts between the monitor and baseline data.

valid for isolated transmission or reflection events

Regularization term (10) plays a dual role in our method: it penalizes oscillatory artifacts in the model difference that may be due to acquisition and computational repeatability issues, and it constrains the inverted model by fitting the sparsest model difference that explains the data. Since problem (9,10) is to a first order equivalent to tomographic model-difference inversion, conceptually we can study the limits of its resolution by considering the constrained tomographic inversion problem

$$\begin{aligned} \|\mathbf{A}\delta\mathbf{s} \; - \; \delta\boldsymbol{\tau}\|_2 \; &< \; \sigma, \\ \|\delta\mathbf{s}\|_0 \; &= \; k, \end{aligned} \tag{11}$$

where $\delta\boldsymbol{\tau}$ is a vector of observed time shifts, $\delta\mathbf{s}$ is the unknown slowness change, $\mathbf{A}$ is the travel-time modeling operator, σ is the 2-norm of the estimated measurement error, and $\|\cdot\|_0$ is the L_0 norm (the number of non-zero components) of a vector. Parameter k in (11) is effectively a sparsity measure of the slowness perturbation. In problem (11) we fit the observed time shifts with a slowness difference of a given sparsity (see Elad (2010) for a discussion of the relation between L_0 and L_1-regularized optimization). If $\delta\mathbf{s}_0$ is a true solution of (11) for some observed time shifts $\delta\boldsymbol{\tau}$, any minimizer $\delta\mathbf{s}$ of (11) satisfies the estimate:

$$\|\delta\mathbf{s} - \delta\mathbf{s}_0\|_2 \; \leq \; \frac{2}{c_{2k}}\sigma, \tag{12}$$

where c_{2K} is the lower restricted isometry constant of operator $\mathbf{A}$ (Candes et al., 2006; Demanet and Nguyen, 2015) defined as

$$c_{2k} \; = \; \min_{J:|J|=2k} \lambda_{\min}\left(\mathbf{A}_J\right), \tag{13}$$

where J is a subset of $2k$ columns of $\mathbf{A}$, $\mathbf{A}_J$ is the operator made up of those columns, $\lambda_{\min}$ is its minimal singular value, and σ is measurement noise. Equation (12) relates recoverability of a $k-$sparse slowness model to acquisition via the isometry constant (13) and noise in the data. Note that simply increasing dimension of the data (the number of receivers) does not improve the estimate (12): the singular value in (13) and the L_2 norm of the noise grow at the same asymptotic rate with the number of receivers so long as noise distribution of an individual time-shift measurement is the same. However, according to the Central Limit Theorem, temporally redundant measurements reduce the noise level: for the temporal average of N repeated measurements at the same receiver locations

$$\delta\boldsymbol{\tau} \; = \; \frac{1}{N}\sum_{i=1}^{N}\delta\boldsymbol{\tau}^i, \tag{14}$$

the corresponding measurement error in the first line of (11) decreases asymptotically as $\sigma/\sqrt[4]{N} \to 0$. In other words, given sufficiently redundant observations, we should be able to recover the geometry and (qualitatively) the magnitude of a sparse model difference. Averaging in (14) does not necessarily mean multiple surveys; we envisage the use of emergent continuous-source technologies (Kurosawa and Kato, 2015) as a

cost-effective alternative to repeated surveys. It should be noted that the magnitude of the subsurface slowness change is recovered qualitatively because the regularization results in a penalization and underestimation of the model difference, however, enhancements exist that can address this phenomenon (Maharramov et al., 2016).

One potentially important implication of estimate (12) for velocity-stress relations of the form (1) is that continuous observations in combination with a robust simultaneous FWI (9,10) can detect relative magnitudes of the subsurface stress changes, such as a "flattening" of (1) for large changes in the effective stress. Our method is merely an inversion tool for detecting small changes in the subsurface, but enhanced monitoring capabilities that can be delivered by this technology open up new, if somewhat speculative at this point, possibilities. For example, can a "flattening" of the velocity-stress curve near a locked fault undergoing stress change due to natural or man-made phenomena indicate an impending slip? While study of viable precursors is well beyond the scope of this work, the inversion technique that we propose may prove instrumental for both conventional and novel techniques of subsurface monitoring.

EXAMPLES

We demonstrate the kind of high-resolution inversion product that can be achieved by our method (9,10) on the synthetic baseline model used by Maharramov et al. (2016). We assume very small velocity changes between first monitor and baseline (Figures 4a,4b) and second and first monitor (Figures 5a,5b).

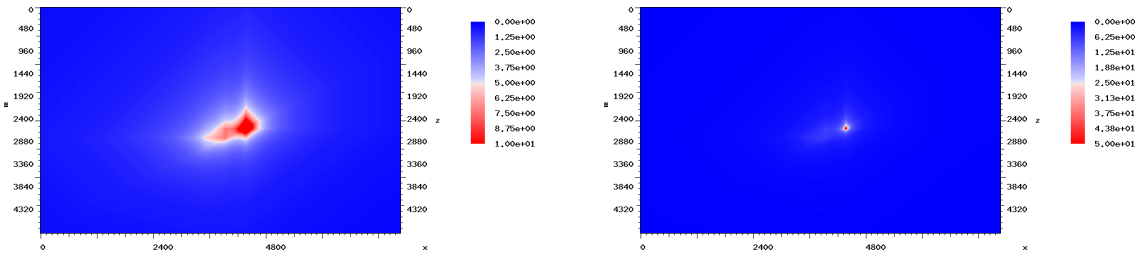

(a) (b)

Figure 4: True model difference between the first monitor and base at 10 (a) and 50 (b) m/s clip. [**CR**]

The figures show the true changes at 10 m/s and 50 m/s clip. The true change is modeled to imitate the stress change near a locked segment of a fault undergoing an interseismic slip, with a singularity near the tip of the locked segment. Note that both compressive and tensile stresses are present around a locked fault segment, and according to (1) that means both positive and negative velocity changes (Segall, 2010). However, in this experiment we extracted only a single positive lobe of the

slowing down of the velocity change rate with increasing stress

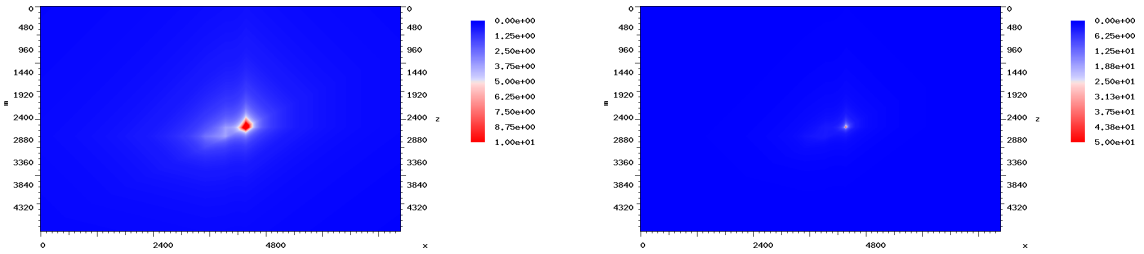

(a) (b)

Figure 5: True model difference between the second and first monitors at 10 (a) and 50 (b) m/s clip. [**CR**]

velocity change. Naive application of FWI often results in non-physical oscillatory artifacts, or "side-lobes", that in our case can be easily mistaken for the effects of stress regime changing from compressive to tensile. Therefore, we demonstrate the robustness of our method (9,10) by recovering a strictly positive velocity-difference anomaly without producing oscillatory artifacts.

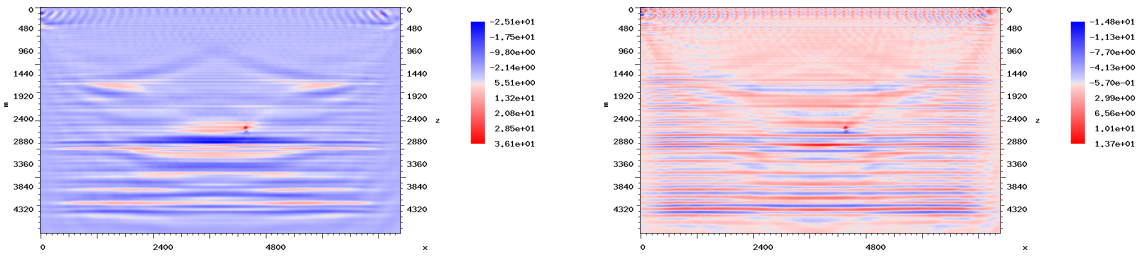

(a) (b)

Figure 6: Parallel-difference inversion of the first (a) and second (b) difference from clean synthetics. [**CR**]

The results of applying a naive parallel-difference FWI to invert the first and second model difference from clean synthetic data are shown in Figures 6a,6b. The clean synthetic was generated using the synthetic model of Maharramov et al. (2016) with 39 shots at 192 m spacing and 320 receivers per shot with a 24 m receiver spacing. Absorbing boundary conditions were applied at the top of the model to avoid surface-related multiples, and a Ricker wavelet centered at 12 Hz was used as the source. FWI was conducted with a frequency continuation from 4 to 20 Hz, starting from a smoothed model of Maharramov et al. (2016). Note that while the parallel-difference FWI resolved location of the stress singularity for both first and second monitor acquisitions, the results are contaminated with oscillatory artifacts of significant magnitude that render them uninterpretable. Solutions of the simultaneous FWI with a TV model-difference regularization for the first and second model

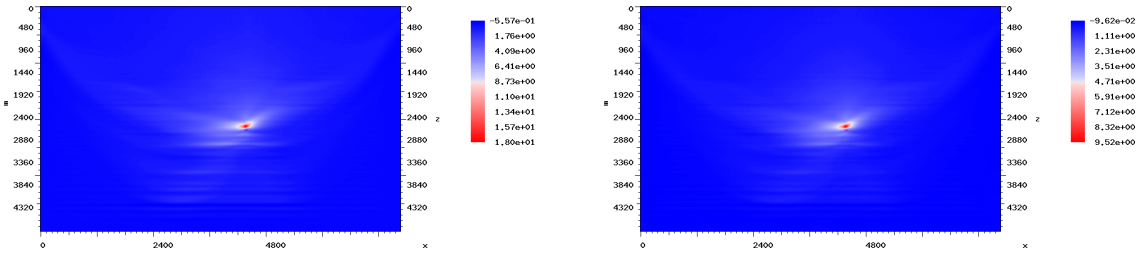

(a) (b)

Figure 7: First (a) and second (b) difference inversion from clean data using simultaneous FWI with a TV model-difference regularization. [**CR**]

differences are shown in Figures 7a,7b. Note that these results are now free of oscillatory artifacts, correctly locate the stress singularity (peak velocity change), and largely recover the velocity difference while indicating their relative magnitudes (see the inverted model differences plotted at 10 m/s clip in Figures 8a,8b).

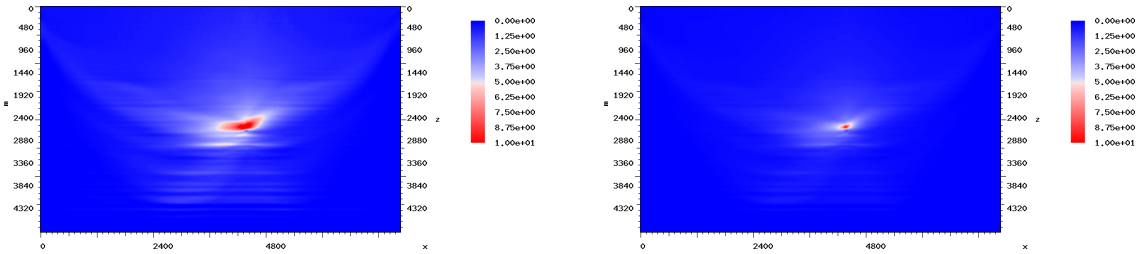

(a) (b)

Figure 8: First (a) and second (b) difference inversion from clean data using simultaneous FWI with a TV model-difference regularization. 10m/s clip [**CR**]

We repeated the same experiment after adding random noise to the data. Signal-to-noise ratio of the noisy data peaked at about 8 dB (see Figure 9) however the signal-to-noise ratio was below 1 outside of the 4-20 Hz range.

The results of a parallel-difference FWI with the same inversion parameters as before are shown in Figures 10a,10b. Note that the second model difference is completely masked by oscillatory artifacts while the difference on the left panel only hints at the location of the stress singularity.

Solving (9,10) with $\mathbf{R} = \nabla$, on the other hand, largely recovered the velocity changes and their relative magnitudes (see Figures 11a,11b), although the absolute magnitudes are underestimated. The TV regularization flattened the velocity peak, resulting in a more ambiguous location of the stress singularity.

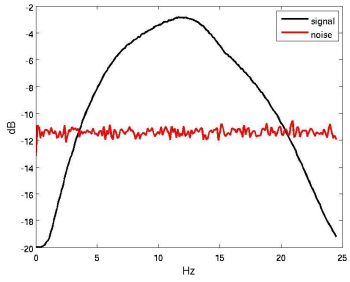

Figure 9: Spectra of the clean data and added noise. [**CR**]

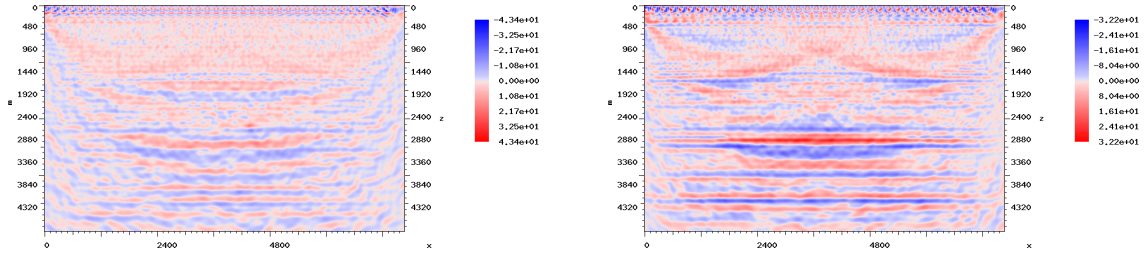

(a) (b)

Figure 10: Parallel-difference inversion of the first (a) and second (b) difference from noisy (right) synthetics. [**CR**]

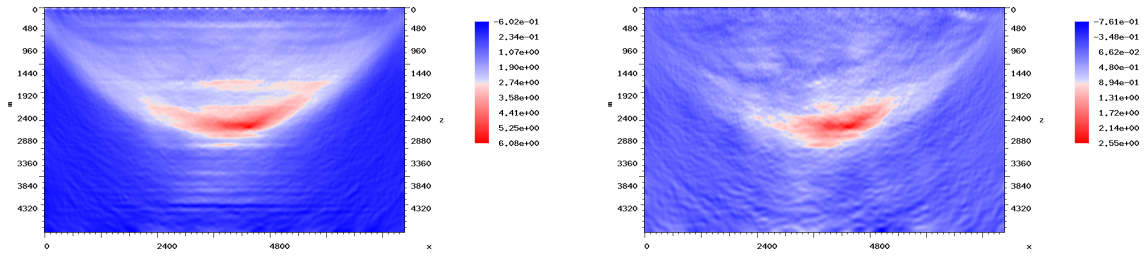

(a) (b)

Figure 11: First (a) and second (b) difference inversion from noisy data using simultaneous FWI with a TV model-difference regularization. [**CR**]

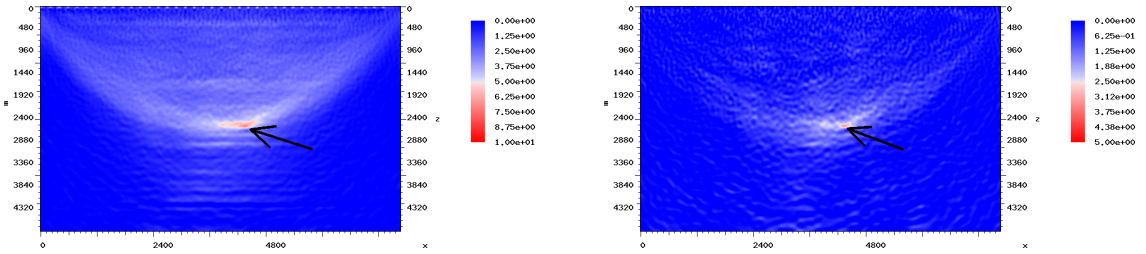

(a) (b)

Figure 12: First (a) and second (b) difference inversion from noisy data using cascaded inversion with a TV and L_1 model-difference regularization. [**CR**]

However, supplying the result of the TV-regularized simultaneous inversion as the starting model for problem (9,10) with a sparsity-promoting L_1 regularization ($\mathbf{R} = \mathbf{I}$ in (10)) results in the recovery of the sparse velocity peak corresponding to the stress singularity—see Figures 12a,12b.

CONCLUSIONS

Given continuous or redundant seismic observations, simultaneous time-lapse FWI with a sparsity-promoting model-difference regularization can be used to detect small changes in the subsurface model induced by changes in the stress field or fluid content. Even in the presence of strong noise, model-difference regularization removes oscillatory artifacts from the inverted model difference while retaining useful information. Cascaded inversion with TV and L_1 regularization helps to achieve multi-scale inversion of subsurface changes, potentially pinpointing locations of significant stress change. While absolute values of the inverted model difference are underestimated due to regularization, relative magnitudes are indicative of changing rates of stress, and may be potentially used in seismic hazard studies.

ACKNOWLEDGEMENTS

The authors would like to thank Paul Segall and Jack Dvorkin for very useful discussions, and Stanford CEEES for computing support.

REFERENCES

Avseth, P., T. Mukerji, and G. Mavko, 2005, Quantitative seismic interpretation: Applying rock physics tools to reduce interpretation risk: Cambridge University Press.

Avseth, P., N. Skjei, and G. Mavko, 2016, Rock-physics modeling of stress sensitivity and 4d time shifts in patchy cemented sandstones application to the visund field, north sea: The Leading Edge, **35**, 868–878.

Candes, E. J., J. Romberg, and T. Tao, 2006, Robust uncertainty principles: exact signal reconstruction from highly incomplete frequency information: IEEE Transactions on Information Theory, **52**, 489–509.

Demanet, L. and N. Nguyen, 2015, The recoverability limit for superresolution via sparsity: arXiv:1502.01385.

Domenico, S. N., 1977, Elastic properties of unconsolidated porous sand reservoirs: Geophysics, **42**, 1339–1368.

Elad, M., 2010, Sparse and redundant representations: Springer.

Estes, C. A., G. Mavko, H. Yin, and T. Cadoret, 1994, Time-lapse inverse scattering theory: SRB Annual Report, **55(B)**, G1–1–G1–9.

Hashin, Z. and S. Shtrikman, 1963, A variational approach to the elastic behavior of multiphase materials: Journal of the Mechanics and Physics of Solids, **11**, 127–140.

Johnston, D., 2013, Practical applications of time-lapse seismic data: Society of Exploration Geophysicists.

Knuth, M. W., H. J. Tobin, and C. Marone, 2013, Evolution of ultrasonic velocity and dynamic elastic moduli with shear strain in granular layers: Granular Matters, **15**, 499–515.

Kurosawa, I. and A. Kato, 2015, Permanent seismic source for continuous reservoir monitoring: Reservoir Monitoring Consortium Semi-Annual Review meeting, University of Southern California.

Lee, M. W., 2003, Elastic properties of overpressured and unconsolidated sediments: U.S. Geological Survey Bulletin, **2214**, 1–14.

Maharramov, M., B. Biondi, and S. Ronen, 2015, Robust simultaneous time-lapse full-waveform inversion with total-variation regularization of model difference: 77th EAGE Conference and Exhibition, Extended Abstract, We P3 09.

Maharramov, M. and B. L. Biondi, 2017, Full waveform inversion for reservoir monitoring—pushing the limits of subsurface resolution: First EAGE Workshop on Practical Reservoir Monitoring, Session: Increasing Value through Processing and Imaging, 6 March 2017, Amsterdam, the Netherlands.

Maharramov, M., B. L. Biondi, and M. A. Meadows, 2016, Time-lapse inverse theory with applications: Geophysics, **81**, R485–R501.

Mavko, G., T. Mukerji, and J. Dvorkin, 2009, The rock physics handbook: Cambridge University Press.

Mindlin, R. D., 1949, Compliance of elastic bodies in contact: Journal of Applied Mechanics, **16**, 259–268.

Prasad, M. and R. Domenico, 1992, Attenuation mechanisms in sands: Laboratory versus theoretical (Biot) data: Geophysics, **57**, 710–719.

Robertson, P. K., S. Sasitharan, J. C. Cunning, and D. C. Sego, 1995, Shear-wave velocity to evaluate in-situ state of Ottawa sand: J. Geotech. Eng., **121**, 262–273.

Rudin, L. I., S. Osher, and E. Fatemi, 1992, Nonlinear total variation based noise removal algorithms: Physica D: Nonlinear Phenomena, **60**, 259–268.

Segall, P., 2010, Earthquake and volcano deformation: Princeton University Press.

Yin, H., 1992, Acoustic velocity and attenuation of rocks: Isotropy, intrinsic anisotropy, and stress induced anisotropy: PhD thesis, Stanford University.

Zimmer, M. A., 2003, Seismic velocities in unconsolidated sands: PhD thesis, Stanford University.